Lattice-distortion Induced Magnetic Transition from Low- temperature Antiferromagnetism to High-temperature Ferrimagnetism in Double Perovskites A 2 FeOsO 6 (A = Ca, Sr)

3 AUTHORS:

Yusheng Hou

Fudan University

5 PUBLICATIONS **1** CITATION

SEE PROFILE

H. J. Xiang

Fudan University

156 PUBLICATIONS **3,358** CITATIONS

SEE PROFILE

Xiaowu Gong

Infineon Technologies

170 PUBLICATIONS **3,829** CITATIONS

SEE PROFILE

SCIENTIFIC REP🞉RTS

Lattice-distortion Induced Magnetic Transition from Low-temperature Antiferromagnetism to High-temperature Ferrimagnetism in Double Perovskites A_2FeOsO$_6$ (A=Ca, Sr)

Y. S. Hou[1], H. J. Xiang[1] & X. G. Gong[1,2]

High-temperature insulating ferrimagnetism is investigated in order to further reveal its physical mechanisms, as well as identify potentially important scientific and practical applications relative to spintronics. For example, double perovskites such as Sr$_2$FeOsO$_6$ and Ca$_2$FeOsO$_6$ are shown to have puzzling magnetic properties. The former is a low-temperature antiferromagnet while the latter is a high-temperature insulating ferrimagnet. In order to understand the underlying mechanisms, we have investigated the frustrated magnetism of A_2FeOsO$_6$ by employing density functional theory and maximally-localized Wannier functions. We find lattice distortion enhances the antiferromagnetic nearest-neighboring Fe-O-Os interaction, however weakens the antiferromagnetic interactions via the Os-O-O-Os and Fe-O-Os-O-Fe paths, so is therefore responsible for the magnetic transition from the low-temperature antiferromagnetism to the high-temperature ferrimagnetism as the decrease of the A^{2+} ion radii. Also discussed is the $5d^3$-$3d^5$ superexchange. We propose that such superexchange is intrinsically antiferromagnetic instead of ferromagnetic as previously thought. Our work clearly illustrates the magnetic frustration can be effectively relieved by lattice distortion, thus paving the way for tuning of complex magnetism in yet other $3d$–$5d$ ($4d$) double perovskites.

Double perovskite oxides A$_2$BB'O$_6$, where A is an alkaline-earth or rare-earth metal and B(B') is a transition metal (TM), have attracted considerable attention due to many recent experimental findings, including those related to room-temperature (RT) half-metallicity[1–5], high-temperature (HT) insulating ferrimagnetism[6–10], multiferroicity[11–14], ferromagnetism[15–17] and so on. Recently, the double perovskites Ca$_2$FeOsO$_6$, SrCaFeOsO$_6$ and Sr$_2$FeOsO$_6$ were found to display dramatically different magnetic behavior[7,18–22]. Ca$_2$FeOsO$_6$ is an insulating ferrimagnet with a very high transition temperature of 320 K[7]. If half of the Ca^{2+} ions of Ca$_2$FeOsO$_6$ were replaced with larger Sr^{2+} ions, the resulting SrCaFeOsO$_6$ was found to retain its ferrimagnetic property, but with a significantly lower Curie temperature of 210 K[18]. However, Sr$_2$FeOsO$_6$ was experimentally found to be an antiferromagnet with low transition temperatures[21]. Experimental observations show that, with the lowering of temperature, Sr$_2$FeOsO$_6$ transforms from the paramagnetic phase to the AF1 antiferromagnetic phase at 140 K, and then to the AF2 antiferromagnetic
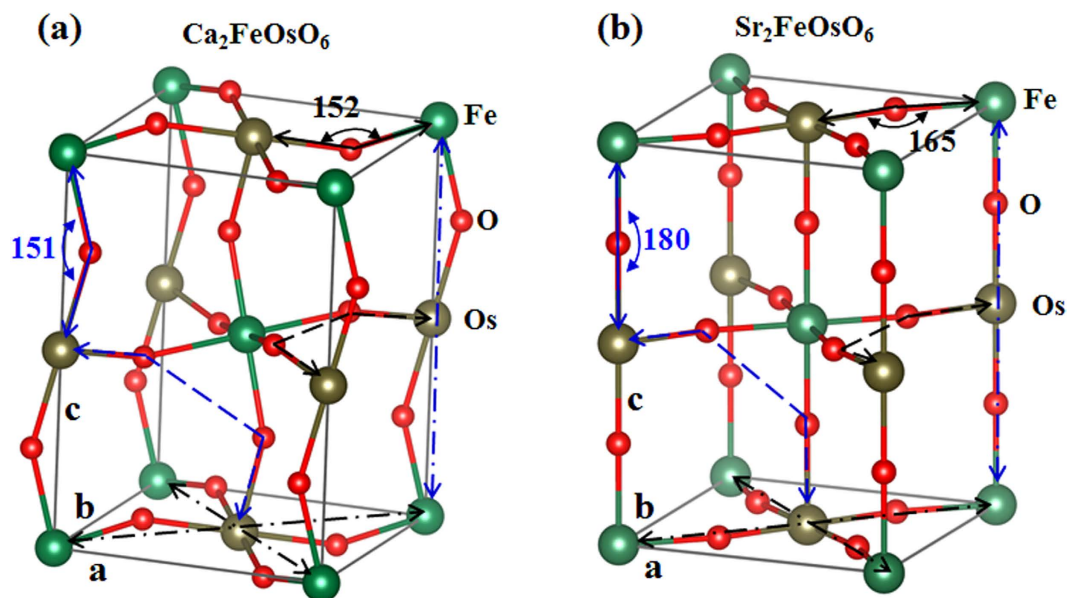
Figure 1. Lattice structures of Ca₂FeOsO₆ (a) and Sr₂FeOsO₆ (b). The Fe-O-Os paths are shown by solid lines, and experimentally measured Fe-O-Os angles are also shown in units of degrees. The Os-O-O-Os paths are depicted by dashed lines. The Fe-O-Os-O-Fe and Os-O-Fe-O-Os paths are depicted by dot-dashed lines. The in-plane and out-of-plane paths are shown in black and blue, respectively. The letter **a**, **b** and **c** denote the crystal axes. Ca²⁺ and Sr²⁺ ions are not displayed for the sake of clarity.

phase at 67 K[21]. These experimental results are particularly interesting because these compounds have similar chemical composition. In this context, many important questions remain.

As a result of spin-lattice coupling, the magnetism is usually correlated with the detailed lattice structure. Previous experiments showed that Ca_2FeOsO_6, $SrCaFeOsO_6$ and Sr_2FeOsO_6 have somewhat different lattice distortion patterns. Ca_2FeOsO_6 crystallizes with a monoclinic space group of $P2_1/n$[7], yet Sr_2FeOsO_6 crystallizes with a tetragonal symmetry[20,21]. In the *ab* plane, the Fe-O-Os, Os-O-O-Os, Fe-O-Os-O-Fe and Os-O-Fe-O-Os paths of Ca_2FeOsO_6 are very similar to those of Sr_2FeOsO_6, except that the lattice distortion in the former case is much stronger (see Fig. 1). In Ca_2FeOsO_6, the out-of-plane Fe-O-Os paths are very bent (see Fig. 1a). Consequently, the out-of-plane Fe-O-Os-O-Fe and Os-O-Fe-O-Os paths are highly distorted as well (see Fig. 1a). However, the out-of-plane Fe-O-Os angles in Sr_2FeOsO_6 are all nicely 180 degrees, and the out-of-plane Fe-O-Os-O-Fe and Os-O-Fe-O-Os paths are not at all distorted (see Fig. 1b). Compared to Ca_2FeOsO_6, Sr_2FeOsO_6 also has less distorted out-of-plane Os-O-O-Os paths. Finally, it is worth noting that $SrCrFeOsO_6$ takes on a similar structure to Ca_2FeOsO_6, but with a reduced structural distortion[7,18]. Therefore, we find progressively weaker lattice distortion when comparing Ca_2FeOsO_6 to $SrCaFeOsO_6$, to Sr_2FeOsO_6.

Although it was pointed out[7] that lattice distortion is correlated with magnetic behavior, the detailed microscopic mechanism remains unclear. Since the generalized double-exchange mechanism operates only in metals[23], it cannot account for the HT insulating ferrimagnetism in Ca_2FeOsO_6. On the other hand, the origin of AF1 and AF2 spin orders of Sr_2FeOsO_6 remains under debate. For the AF1 order, it is widely accepted that the ferrimagnetic (FIM) *ab* planes are coupled to the neighboring planes by the out-of-plane ferromagnetic (FM) Fe-O-Os superexchange[20,22]. However, it has been recently suggested that these FIM *ab* planes may be coupled by out-of-plane antiferromagnetic (AFM) Os-O-O-Os interactions[18]. For the AF2 order, Morrow *et al.* proposed that the long-range Fe-Fe AFM interaction (via the four-bond Fe-O-Os-O-Fe path) dominates, and produces AFM-type Fe-Os chains along the *c* axis[18], however Kanungo *et al.* showed that the long-range Os-Os AFM interaction through the four-bond Os-O-Fe-O-Os path is primarily responsible[22]. For the magnetic ordering temperature, there is to date no clear quantitative understanding as to why the T_N of AF1 is unexpectedly low. To the best of our knowledge, there also remains a lack of clear understanding as to how LT antiferromagnetism of A_2FeOsO_6 transforms to HT ferrimagnetism with an accordant increase in lattice distortion, namely, with a decrease in the ionic radii of A^{2+} ions.

In this Report, in order to obtain a comprehensive insight into the magnetic behaviors of A_2FeOsO_6 (A = Ca, Sr), we systematically investigate the frustrated magnetism of the double perovskites Ca_2FeOsO_6, $SrCaFeOsO_6$ and Sr_2FeOsO_6 by employing density functional theory (DFT) and maximally-localized Wannier functions (MLWFs). We find lattice distortion enhances the AFM Fe-O-Os interaction but weakens the AFM interactions of the Os-O-O-Os and Fe-O-Os-O-Fe paths. As a result of the serious lattice distortion, Ca_2FeOsO_6 has a strong and dominant AFM interaction between the nearest

neighboring (NN) Fe^{3+} and Os^{5+} ions. Consequently, the NN Fe^{3+} and Os^{5+} ions are coupled antiparallel and ferrimagnetism is experimentally observed. Simultaneously, corresponding AFM interactions via the Os-O-O-Os and Fe-O-Os-O-Fe paths are weak, so the Os-Os and Fe-Fe induced magnetic frustration is effectively relieved, and one observes a very high T_C. Because $SrCaFeOsO_6$ is less distorted compared to Ca_2FeOsO_6, its magnetic frustration becomes stronger despite the FIM ground state being preserved. Accordingly, its T_C is lowered. In the tetragonal $I4/m$ structure of Sr_2FeOsO_6, lattice distortion vanishes along the c axis but it is very similar to that of Ca_2FeOsO_6 in the ab plane. This special lattice distortion pattern results in both the in-plane NN Fe^{3+} and Os^{5+} ions being aligned antiparallel and the FM chains along the c axis. The resulting magnetic structure is just the strongly frustrated antiferromagnetism AF1 with a very low Neel temperature T_N^{AF1}. Lastly, strong spin-lattice coupling leads to a transformation from AF1 to AF2. Our work illustrates the magnetic frustration can be effectively relieved by lattice distortion, which may well be responsible for the complex magnetism observed in other $3d$–$5d$ ($4d$) double per-ovskites as well.

Results

Lattice-Distortion dependence of magnetic interactions in Ca_2FeOsO_6.

In order to understand why Ca_2FeOsO_6 is FIM, and how lattice distortion affects this ferrimagnetism, we have systematically explored the effect of lattice distortion on the magnetic interaction of Ca_2FeOsO_6. Since the positions of O^{2-} ions are known to be vital, we performed a series of calculations using a linear superposition of the Wyckoff positions of the O^{2-} ions of both the relaxed and pseudo-cubic structure. In the pseudo-cubic structure, O^{2-} ions are artificially positioned to make Fe-O-Os angles straight, but lattice constants and the positions of the Fe^{3+}, Os^{5+} and Ca^{2+} ions are fixed at their corresponding positions in the relaxed structure. The O^{2-} ions positions is computed as follows:

$$\boldsymbol{R}(\alpha_x) = (1 - \alpha_x)\boldsymbol{R}^{relax} + \alpha_x\boldsymbol{R}^{cubic}. \tag{1}$$

In Eq. (1), $\boldsymbol{R}^{relax}$ and $\boldsymbol{R}^{cubic}$ are the position vectors of O^{2-} ions in the relaxed and pseudo-cubic structures respectively, and α_x varies between 0 and 1. For example, $\alpha_x = 0$ corresponds to the relaxed structure and $\alpha_x = 1$ corresponds to the pseudo-cubic structure. Thus α_x characterizes the lattice distortion induced by O^{2-} ions. The dominant magnetic interactions are divided into three groups (see Fig. 2a). The first group is the superexchange between the NN Fe^{3+} and Os^{5+} ions. The second involves super-superexchange between the next near-neighboring (NNN) Os^{5+} ions. The third involves long-range Fe-Fe interactions via the four-bond Fe-O-Os-O-Fe path. Technically, we adopt the four-state mapping method to evaluate these various magnetic interactions[24]. Note that a positive exchange constant J corresponds to the AFM interaction, but a negative exchange constant J corresponds to the FM interaction.

We find the magnetic interaction between the NN Fe^{3+} and Os^{5+} ions is intrinsically AFM. The calculated magnetic exchange constants of Fe-O-Os paths in the pseudo-cubic structure are shown in the Fig. 2b. They are all positive and thus AFM. The intrinsically AFM interaction of the Fe-O-Os path can be qualitatively understood based upon the extended Kugel-Khomskii model[25-27]. According to this model, magnetic interactions can be evaluated based on the hopping integrals and on-site energies, namely,

$$J_{ij} = J_{ij}^{AFM} + J_{ij}^{FM} = \sum_{afm}\frac{4t_{ij}^{afm} \cdot t_{ij}^{afm}}{\left(U + \Delta_{ij}\right)} - \sum_{fm}\frac{4t_{ij}^{fm} \cdot t_{ij}^{fm} \cdot J_H}{\left(U + \Delta_{ij}\right)\left(U + \Delta_{ij} - J_H\right)}. \tag{2}$$

In Eq. (2), U, J_H and Δ_{ij} are the on-site Coulomb interaction, Hund's coupling and the energy difference between the ith and j^{th} energy levels, respectively, and $t_{ij}^{afm}\left(t_{ij}^{fm}\right)$ is the hopping integral. The first term in J_{ij} describes the AFM contribution due to the hybridization between the two occupied orbitals. The second term describes the FM contribution due to the hybridization between the occupied and empty orbitals. In order to elucidate why the magnetic interaction between the NN Fe^{3+} and Os^{5+} ions is intrinsically AFM, we take the Fe-O-Os path along the c axis of the pseudo-cubic Ca_2FeOsO_6 as a typical example. Its detailed hopping integrals and energy levels are given in the right panel of Fig. S1 of supplemental material (SM). Compared with the FM interaction between the NN Mn^{3+} ions in the cubic $LaMnO_3$ (LMO)[28], two pivotal factors are seen to drive the magnetic interaction between the NN Fe^{3+} and Os^{5+} ions in the pseudo-cubic Ca_2FeOsO_6 to be intrinsically AFM. The first factor is the very large energy difference Δ (up to 3.0 eV) between the occupied e_g orbitals of Fe^{3+} ion and the unoccupied e_g orbitals of Os^{5+} ion. This will give a weak FM contribution according to the Eq. (2). The second factor is the rather large hopping integrals between the occupied t_{2g} orbitals of the Fe^{3+} and the Os^{5+} ions. For instance, the leading hopping integral is 0.27 eV. This will give strong AFM contribution according to the Eq. (2). Therefore the AFM contribution dominates over the FM one, giving rise to the intrinsically AFM interaction between the NN Fe^{3+} and Os^{5+} ions, regardless of the magnitude of the Fe-O-Os angle.

In addition, we find lattice distortion can effectively relieve the magnetic frustration in Ca_2FeOsO_6 and thereby raise its FIM phase transition temperature T_C. Since Os^{5+} ions form a face-centered sublat-tice with geometrically frustrated edge-sharing tetrahedrons, antiferromagnetically interacting Os^{5+} ions
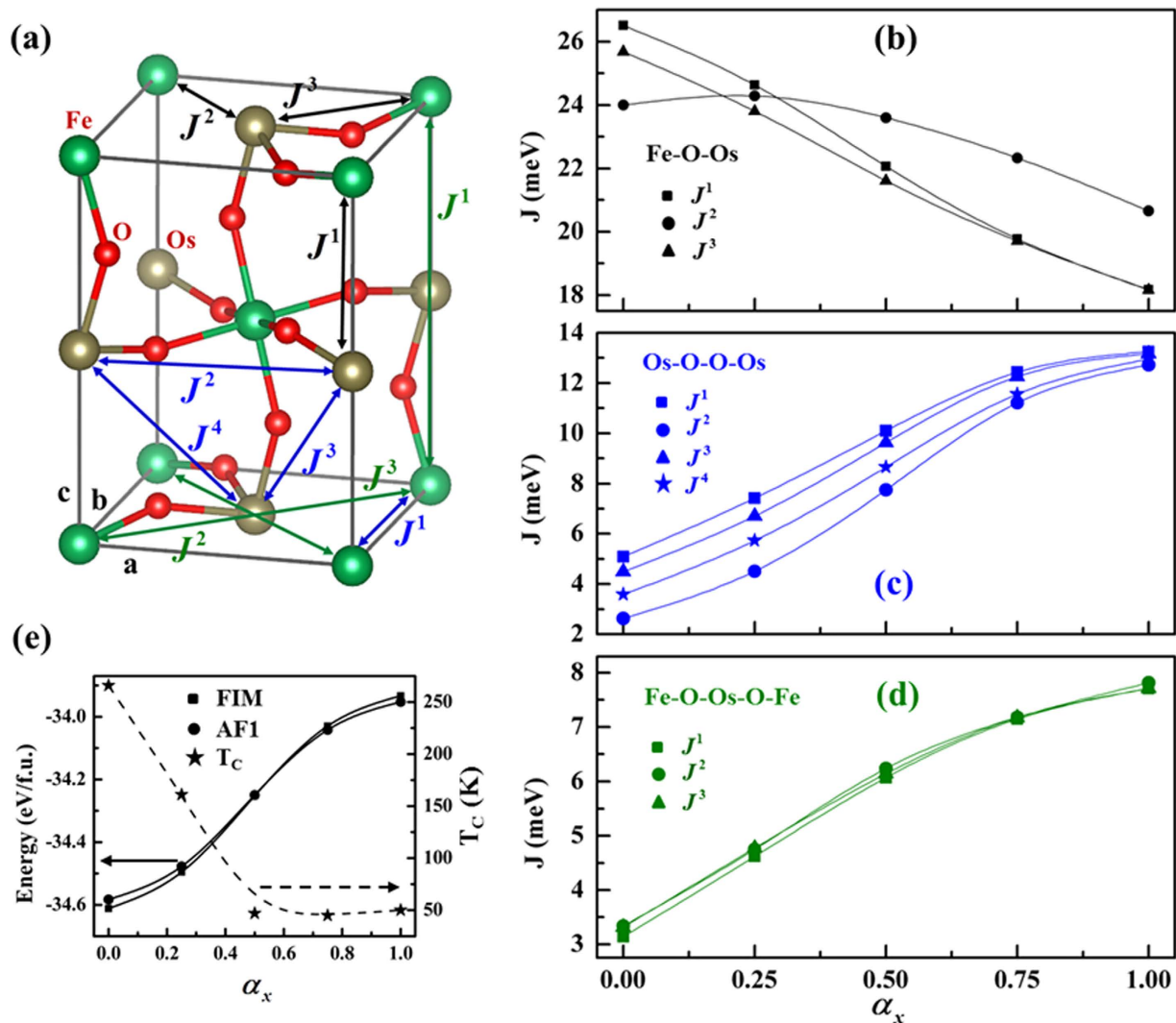
Figure 2. Magnetic exchange paths and evolutions of magnetic interactions and T_C of Ca_2FeOsO_6. (a)
The NN superexchange paths Fe-O-Os (marked by the black J^1, J^2 and J^3), NNN super-superexchange paths
Os-O-O-Os (marked by the blue J^1, J^2, J^3 and J^4) and long-range four-bond Fe-O-Os-O-Fe exchange paths
J^1_{Fe-Fe}, J^2_{Fe-Fe} and J^3_{Fe-Fe} (marked by the green J^1, J^2 and J^4) are shown by the black, blue and green solid
lines, with double arrowheads respectively. The dependence of Fe-O-Os superexchange interactions, Os-O-
O-Os super-superexchange interactions, and the long-range four-bond Fe-O-Os-O-Fe magnetic interactions
on the lattice distortion (α_x) are shown in (**b–d**), respectively. Figure (**e**) shows the evolution of T_C (star)
obtained by Monte Carlo and the energy of the FIM (square) and AF1 (circle) magnetic structures with
respect to lattice distortion (α_x).

are strongly frustrated. Figure 2c shows lattice distortion can dramatically weaken the NNN AFM inter-
actions between the NNN Os^{5+} ions, which implies that the Os^{5+} ions' induced magnetic frustration can
be relieved by lattice distortion. Besides, Fe^{3+} ions can also be magnetically frustrated because of the
following factor. The dominant NN Fe-O-Os AFM interactions require the magnetic moments of Fe^{3+}
ions to be aligned parallel, but the AFM magnetic interaction through the four-bond Fe-O-Os-O-Fe
paths requires the magnetic moments of Fe^{3+} ions to be antiparallel. Because lattice distortion slightly
enhance the NN AFM interactions between the NN Fe^{3+} and Os^{5+} ions (see Fig. 2b) but weakens the
long-range four-bond Fe-O-Os-O-Fe AFM interactions along the pseudo-cubic [001], [010] and [100]
axes (see Fig. 2d), it can effectively relieve the Fe^{3+} ions induced magnetic frustration. And, we should
note, accompanied with the relief of such magnetic frustration is the raising of the FIM phase transition
temperature T_C. Figure 2e shows the evolution of T_C obtained by Monte Carlo (MC) as lattice distortion
weakens. It clearly shows the T_C of the relaxed structure ($\alpha_x = 0$) (about 266 K, close to the experimen-
tally measured one[7] $T_C \approx 320$ K) is higher than that of the less distorted one ($\alpha_x = 0.25$). Note that T_C
slightly increases with the weakening of lattice distortion for large α_x. This is because the magnetic
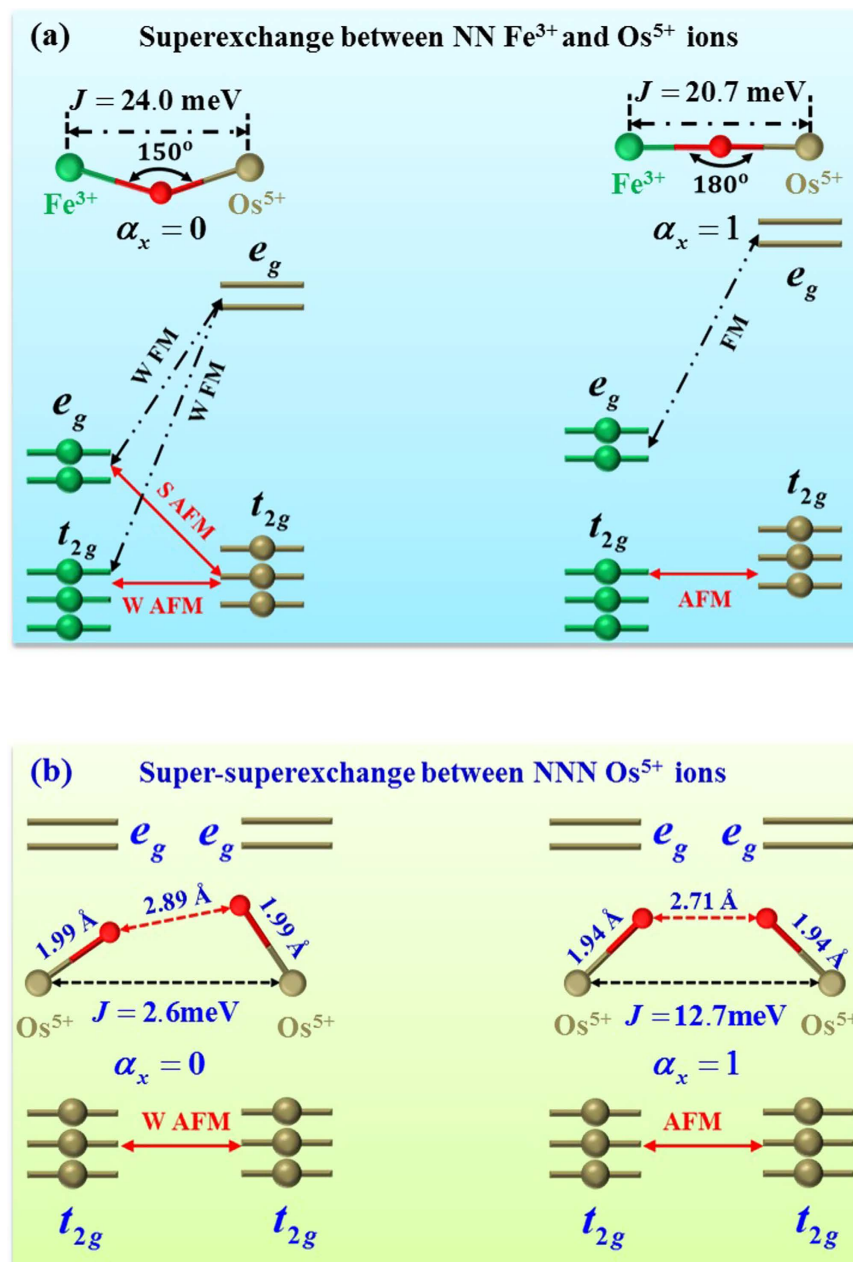
Figure 3. Mechanism by which lattice distortion enhances the NN AFM interaction between Fe^{3+} and Os^{5+} ions (a), and weakens the NNN AFM interaction between Os^{5+} ions (b) in Ca_2FeOsO_6. Solid (dashed) lines with double arrowheads indicate the electron hopping causing AFM (FM) contribution to the NN superexchange or NNN super-superexchange. S and W represent "strong" and "weak" words, respectively. In (a), the FM contribution of $a_x = 0$ is weaker than that of $a_x = 1$. However, the AFM contribution of $a_x = 0$ is stronger than that of $a_x = 1$. In (b), the AFM contribution of $a_x = 0$ is weaker than that of $a_x = 1$. Insets in (a,b) are for the local structures of Fe-O-Os and Os-O-O-Os paths, respectively. The relevant bond angles, bond lengths and calculated magnetic exchange constants are explicitly given in the inset of figures (a) and (b).

ground state of Ca_2FeOsO_6 with small lattice distortion is no longer FIM but AFM with the AF1 order as appearing in the Sr_2FeOsO_6 (see Fig. 2e).

Figure 3a demonstrates the mechanism by which lattice distortion enhances the NN Fe-O-Os AFM interaction. For illustration purposes, we consider the Fe-O-Os path along the c axis as an example. Fig. S1 of the SM shows the detailed leading hopping integrals and energy levels in the relaxed and pseudo-cubic structures, respectively. These hopping integrals clearly indicate lattice distortion tremendously reduces the electron hopping between the occupied e_g orbitals of Fe^{3+} ions and the unoccupied one of Os^{5+} ions. Consequently, one can conclude based on the formula of J_{ij} (see Eq. (2)) that lattice

distortion extraordinarily reduces the FM contribution to the NN superexchange. In contrast, lattice distortion has a rather minor effect on the AFM contribution, because it increases the electrons hopping between the occupied e_g orbitals of Fe^{3+} ions and the occupied t_{2g} orbitals of Os^{5+} ions, although it reduces the hopping between the occupied t_{2g} orbitals of Fe^{3+} and Os^{5+} ions. Therefore, lattice distortion enhances the NN AFM interaction by dramatically reducing the FM contribution, and by maintaining the AFM contribution almost unchanged.

We find the NNN AFM interaction between the NNN Os^{5+} ions is weakened by lattice distortion. This is because such NNN super-superexchange has a sensitive dependence on the geometry of the Os-O-O-Os path. Shown in the insets of Fig. 3b are the geometries of the relevant Os-O-O-Os paths in the relaxed and pseudo-cubic structures. The detailed leading hopping integrals and energy levels between the investigated Os^{5+} ions are shown in the Fig. S2 of the SM. Note that FM contribution to the NNN super-superexchange is rather weak in the relaxed and pseudo-cubic structures because of small hopping integrals and large energy differences. So the NNN super-superexchange is basically determined by the AFM contribution. Comparison of the two investigated Os-O-O-Os paths shown in Fig. 3b clearly indicates lattice distortion increases the O-O bond length. Such an increase can reduce the hopping between the t_{2g} electrons of Os^{3+} ions, as is readily verified by the reduction of hopping integrals from the pseudo-cubic structure to the relaxed one (see Fig. S2 of the SM). Therefore lattice distortion blocks the t_{2g} electron hopping through Os-O-O-Os path, thereby weakening the otherwise robust NNN AFM interaction.

Low-temperature antiferromagnetism of Sr_2FeOsO_6.

Sr_2FeOsO_6 adopts two different magnetic and lattice structures depending on temperature[21]. With decreasing temperature, its magnetic structure transforms from AF1 into AF2 antiferromagnetism and its lattice structure transforms from $I4/m$ into $I4$ with a dimerization between the NN Fe^{3+} and Os^{5+} ions along the c axis. In both AF1 and AF2, moments of Fe^{3+} and Os^{5+} ions are coupled antiparallel in the ab plane (Fig. 4a and Fig. 4c). In AF1 spins order as $++++$ along the c axis (Fig. 4b). In AF2, spins order as $++--++--$ (Fig. 4d).

Our study on the $I4/m$-AF1 phase (Fig. 4a and Fig. 4b) shows that the out-of-plane NN AFM interaction (J^2_{Fe-Os}) is much weaker than its in-plane counterpart (J^1_{Fe-Os}) and that the out-of-plane NNN AFM interaction (J^2_{Os-Os}) is stronger than the in-plane counterpart (J^1_{Os-Os}), which are readily understood based upon our above results for Ca_2FeOsO_6. Because the Fe-O-Os angle along the c axis is 180.0°, similar to that in pseudo-cubic Ca_2FeOsO_6, the out-of-plane NN AFM interaction J^2_{Fe-Os} is weak. In the tetragonal ab plane, lattice distortion is similar to that in the relaxed Ca_2FeOsO_6, so the in-plane NN AFM interaction J^1_{Fe-Os} is strong. The weak in-plane NNN AFM interaction J^1_{Os-Os} is due to the strong in-plane lattice distortion blocking the Os^{5+} ions' t_{2g} electron hopping, similar to the weak NNN AFM interactions in the relaxed Ca_2FeOsO_6. Besides, the out-of-plane NNN AFM interaction J^2_{Os-Os} is stronger than that of the relaxed Ca_2FeOsO_6 but weaker than that of the pseudo-cubic Ca_2FeOsO_6. Overall, such magnitudes of the spin interactions are a result of the combination of the absence of the lattice distortion along the c axis and the strong lattice distortion in the tetragonal ab plane. Finally, it is expected that the long-range four-bond Fe-O-Os-O-Fe AFM interaction along the c axis ($J^3_{Fe-Fe} = 6.2$ meV) is stronger than the in-plane counterpart ($J^2_{Fe-Fe} = 5.1$ meV). Note that the super-superexchange Fe-Fe interaction J^1_{Fe-Fe} through the Fe-O-O-Fe path is very weak ($J^1_{Fe-Fe} = 1.0$ meV) compared with the others, and thus is omitted from our model.

Here we discuss how the competing magnetic interactions establish AF1 in the tetragonal $I4/m$ structure of Sr_2FeOsO_6. First, it should be noted that the magnetic easy axis is the c axis[21], that is, magnetic moments can only point up and down along it. The calculated results (see Fig. 4a) show that the in-plane NN AFM interaction J^1_{Fe-Os} is approximately four times of the magnitude of the in-plane NNN AFM interaction J^1_{Os-Os}, as well as the in-plane long-range four-bond Fe-O-Os-O-Fe AFM interaction J^2_{Fe-Fe}. In addition, their pairwise numbers (Z's) are all the same ($Z=4$). For the in-plane magnetic interactions, therefore, the optimal configuration is such that the magnetic moments of Fe^{3+} and Os^{5+} ions are aligned antiparallel in the ab plane, as experimental observations[21]. For the magnetic interaction along the c-axis, the out-of-plane NN (J^2_{Fe-Os}), NNN (J^2_{Os-Os}) and the long-range four-bond (J^3_{Fe-Fe}) magnetic interactions are all AFM (see Fig. 4b). If only the out-of-plane NN AFM interaction J^2_{Fe-Os} is taken into consideration, the FIM Fe^{3+}-Os^{5+} layers should be coupled antiparallel along the c axis. In this case, the resulting magnetic structure is FIM (see Fig. 5a). If only the out-of-plane NNN AFM interaction J^2_{Os-Os} is taken into consideration, the FIM Fe^{3+}-Os^{5+} layers should be coupled parallel along the c axis. In this case, the resulting magnetic structure is AF1 (Fig. 5b), which is just the experimentally observed. Finally, if only the long-range four-bond Fe-O-Os-O-Fe AFM interaction J^3_{Fe-Fe} is taken into consideration, it gives rise to AF2 (Fig. 5c). Obviously, the out-of-plane NN (J^2_{Fe-Os}), NNN (J^2_{Os-Os}) and the long-range four-bond (J^3_{Fe-Fe}) AFM interactions compete to give rise to the different magnetic ground states. Since their magnitudes are comparable, their pairwise numbers are the decisive factor in determining the optimal magnetic structure, being $Z_{NN}=2$, $Z_{NNN}=8$ and $Z_{Fe-O-Os-O-Fe}=2$, respectively. This indicates the out-of-plane NNN AFM interaction J^2_{Os-Os} easily dominates the out-of-plane NN J^2_{Fe-Os} and long-range four-bond J^3_{Fe-Fe} AFM interactions. Therefore the optimal magnetic configuration is AF1.

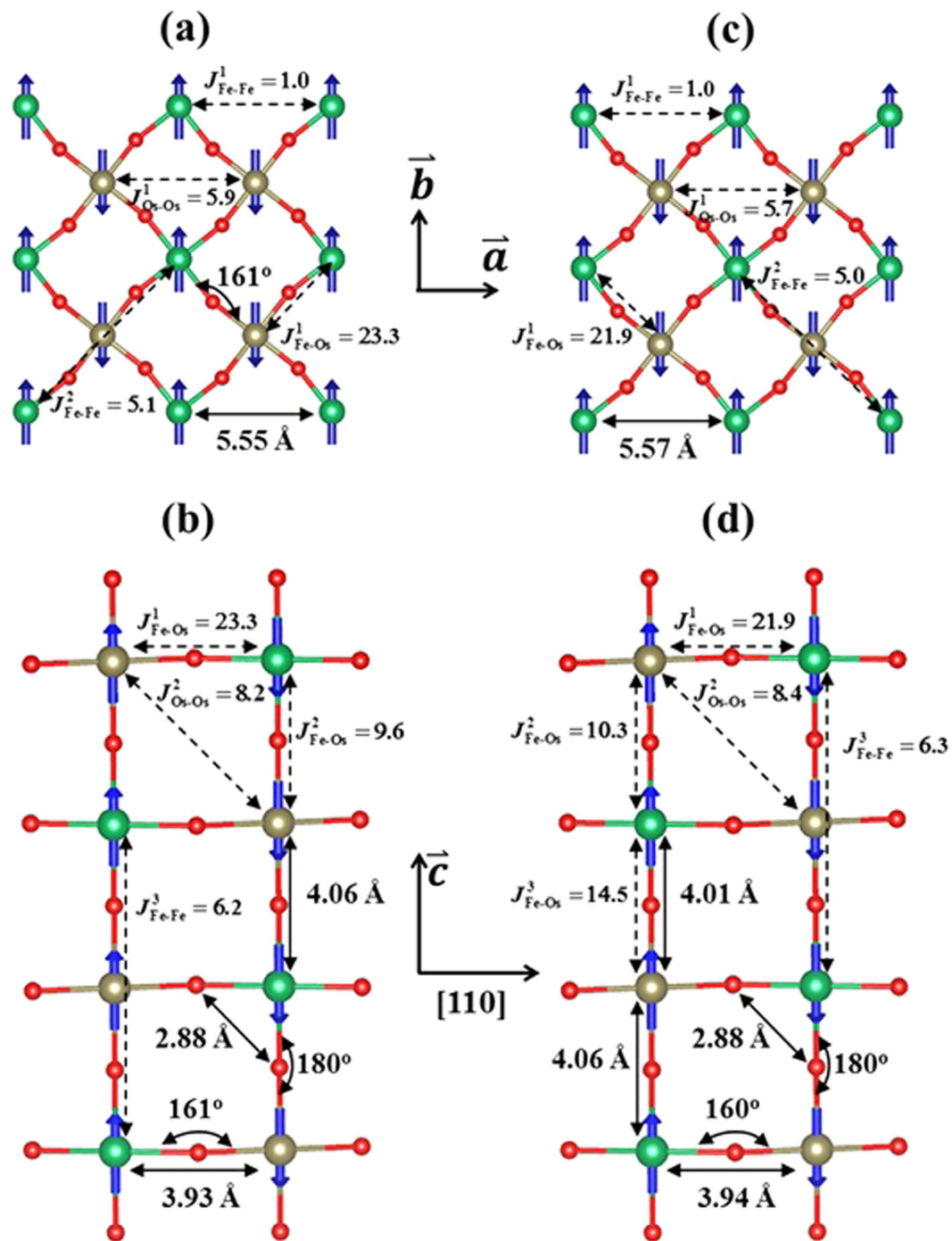**Figure 4. Dominant magnetic exchange paths and AF1, AF2 magnetic structures of Sr$_2$FeOsO$_6$.** All magnetic exchange constants J are in units of meV. Figures (**a,b**) correspond to the $I4/m$-AF1 phase. Figures (**c,d**) correspond to the $I4$-AF2 phase. Figures (**a,c**) are the spin arrangement in the tetragonal ab plane. Figures (**b,d**) are the spin ordering along the c axis. Blue arrows represent spins. The relevant bond distances and angles obtained from DFT calculations are shown in (**a–d**).

This deduction can be confirmed as follows. In the FIM, all the out-of-plane Fe-Fe and Os-Os pairs are frustrated (see Fig. 5a). In the AF1, all the out-of-plane Fe-Os and Fe-Fe pairs are frustrated (see Fig. 5b). In the AF2, half of the out-of-plane Fe-Os and Os-Os pairs are frustrated (see Fig. 5c). In terms of the out-of-plane NN J^2_{Fe-Os}, NNN J^2_{Os-Os} and long-range four-bond J^3_{Fe-Fe} AFM interactions, therefore, the formula-unit (f.u.) magnetic energies of the FIM, AF1 and AF2 are as follows:
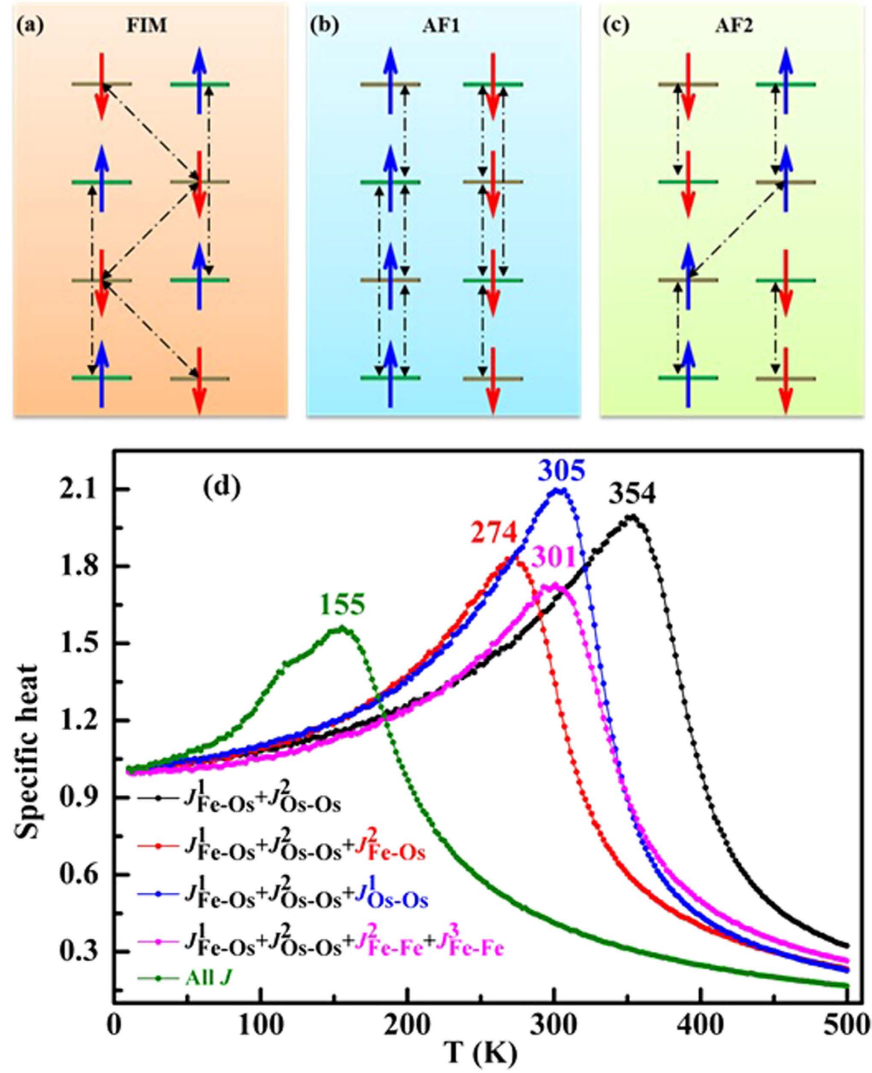
Figure 5. FIM (**a**), AF1 (**b**) and AF2 (**c**) magnetic structures. In (**a–c**), the frustrated magnetic ions pairs are connected by black dashed lines with double arrowheads. Fe (Os) sites are represented by the green (gray) horizontal lines. Blue (red) arrows represent up (down) spins. Figure (**d**) shows the specific heat of Sr_2FeOsO_6, calculated as a function of temperature T in terms of spin exchange interactions. The peak locates the magnetic phase transition temperature T_N.

$$E_{FIM}(J) = -2J_{Fe-Os}^2 + J_{Fe-Fe}^3 + 4J_{Os-Os}^2 = 19.8\,\text{meV/f.u.} \quad (3)$$

$$E_{AF1}(J) = 2J_{Fe-Os}^2 + J_{Fe-Fe}^3 - 4J_{Os-Os}^2 = -7.4\,\text{meV/f.u.} \quad (4)$$

$$E_{AF2}(J) = -J_{Fe-Fe}^3 = -6.2\,\text{meV/f.u.} \quad (5)$$

This indicates that FIM should have the highest energy, with AF2 at a median value, then AF1 at the lowest level. Such estimation is in accord with our DFT calculations: $E_{FIM} = -34.139\,\text{meV/f.u.}$ $> E_{AF2} = -34.153\,\text{meV/f.u.} > E_{AF1} = -34.156\,\text{meV/f.u.}$ So AF1 is found to readily relieve magnetic frustration.

The low Neel temperature T_N of the AF1 is a result of the strong magnetic frustration. Actually, only the in-plane J_{Fe-Os}^1 and the out-of-plane J_{Os-Os}^2 AFM interactions are not frustrated in the AF1. However, the in-plane J_{Os-Os}^1, out-of-plane J_{Fe-Os}^2 and the long-range four-bond J_{Fe-Fe}^2, J_{Fe-Fe}^3 AFM interactions antagonize the AF1 antiferromagnetism, and therefore will induce frustration. Our MC simulations (see Fig. 5d) indicate the T_N of AF1 is very high, up to 354 K, sharply contradicting with the experimentally observed value (140 K), if only J_{Fe-Os}^1 and J_{Os-Os}^2 are taken into consideration. To determine why the

experimentally measured T_N is so low, we performed four additional MC simulations: one with the in-plane J^1_{Os-Os}, one with the out-of-plane J^2_{Fe-Os}, one with the long-range four-bond J^2_{Fe-Fe} and J^3_{Fe-Fe}, and one with all of these magnetic interactions. The resulting specific heat versus temperature plots are presented in Fig. 5d. As can be seen, J^1_{Os-Os}, J^2_{Fe-Os} and the long-range four-bond J^2_{Fe-Fe} and J^3_{Fe-Fe} can all lower the T_N because they are all frustrated. Moreover, the out-of-plane Fe-O-Os AFM interactions make the largest contribution to the lowering of T_N for AF1. If all the dominating magnetic interactions are taken into consideration, the MC simulated T_N is 155 K, which is very close to the experimental value.

By comparing the magnetic exchange constants of $I4$ structure with those of $I4/m$ structure (see Fig. 4), one finds that the magnetic interactions in the former are very similar to the latter's, with the exception that the rather slight dimerization along the c axis in the $I4$ structure prominently enhances the out-of-plane NN AFM interactions J^3_{Fe-Os} (see Fig. 4d), which indicates a very strong spin-lattice coupling. Like in the $I4/m$ structure, the long-range four-bond Fe-O-Os-O-Fe AFM interaction J^3_{Fe-Fe} favors the formation of the AF2, as does the enhancement of the out-of-plane J^3_{Fe-Os}. Thus we attribute the AF2 antiferromagnetism in $I4$ structure to the strong spin-lattice coupling.

Low-temperature ferrimagnetism in the SrCaFeOsO$_6$.

Comparing SrCaFeOsO$_6$ with Sr$_2$FeOsO$_6$ and Ca$_2$FeOsO$_6$, one can conclude that its mediate lattice distortion causes its ferrimagnetism to have a lower T_C. Experiments show that SrCaFeOsO$_6$ has a rather similar lattice structure to that of Ca$_2$FeOsO$_6$[18]. However, its Fe-O-Os bond angles reveal a more linear geometry than that of Ca$_2$FeOsO$_6$, because half of Ca^{2+} ions are replaced by larger Sr^{2+} ions[18]. So it can be inferred that SrCaFeOsO$_6$ can be readily ferrimagnetic. To confirm this, we studied three different types of arrangements of Ca^{2+} and Sr^{2+} ions. The first is where all the Ca^{2+} (Sr^{2+}) are arranged in the ab plane (Fig. 6a). The second is where all Ca^{2+} (Sr^{2+}) are arranged along the c axis (Fig. 6b). The third is where Ca^{2+} and Sr^{2+} ions are arranged in a checkerboard manner (Fig. 6c). For each arrangement, the FIM, AF1 and AF2 are considered. In all three of these cases, FIM always has the lowest total energy (see Fig. 6d). So the magnetic ground of SrCaFeOsO$_6$ should be FIM, consistent with experimental observations[18]. Since its Fe-O-Os bond becomes straighter, its NN Fe-O-Os AFM interactions become weaker however its NNN Os-O-O-Os and long-range four-bond Fe-O-Os-O-Fe AFM interactions become stronger. This is verified by the calculated magnetic exchange parameters, as listed in the Table I of the SM. Consequently, its magnetic frustration gets stronger and its T_C should accordingly be lowered. Our MC simulated T_C for SrCaFeOsO$_6$ is approximately 100 K, lower than the corresponding T_C of 266 K for Ca$_2$FeOsO$_6$, consistent with experimental observations.

Discussions

Based on the present work, an important and general rule on the $3d^5$–$5d^3$ superexchange in the double perovskites can be proposed as follows. It is generally accepted that[29] the d^5-d^3 superexchange changes from FM for $\theta > \theta_c$ to AFM for $\theta < \theta_c$ with $135° < \theta_c < 150°$. However, we demonstrate the magnetic interaction between $3d^5$ and $5d^3$ TMs will be intrinsically AFM (this conclusion is independent of the particular choice of (a reasonable) U, see Table II of the SM) and further that this AFM interaction will increase as its angle θ decreases, as evidenced by the Fe-O-Os interactions in Ca$_2$FeOsO$_6$, SrCaFeOsO$_6$ and Sr$_2$FeOsO$_6$. This intrinsically AFM interaction results from both the large hopping integrals between the occupied t_{2g} orbitals and the large energy difference between the occupied e_g orbitals of $3d$ TM, and the unoccupied orbitals of $5d$ TM, because the former gives rise to a strong AFM contribution and the latter gives rise to a relatively weak FM contribution to the $3d^5$–$5d^3$ superexchange. As the angle θ decreases, the electron hoppings between the occupied e_g orbitals of the $3d^5$ TM and the unoccupied ones of the $5d^3$ TM will be substantially reduced, but the electron hopping between the occupied orbitals of $3d^5$ TM and $5d^3$ TM remain largely unchanged. Thus decreasing the angle θ means reducing the FM contribution, while leaving the AFM contribution largely unchanged. Consequently, the AFM interaction of the $3d^5$-O-$5d^3$ path increases with decreasing θ.

Conclusions

In conclusion, we have investigated the effect of lattice distortion on the frustrated magnetism of certain double perovskites: Ca$_2$FeOsO$_6$, Sr$_2$FeOsO$_6$ and Sr$_2$CrOsO$_6$. In these cases, we find lattice distortion enhances the NN AFM Fe-O-Os interactions but weakens the AFM interactions of the Os-O-O-Os and Fe-O-Os-O-Fe paths. Because lattice distortions become increasingly severe from Sr$_2$FeOsO$_6$ to SrCaFeOsO$_6$ to Ca$_2$FeOsO$_6$, the NN AFM Fe-O-Os interactions also become increasingly strong, but the AFM interactions of Os-O-O-Os and Fe-O-Os-O-Fe paths become increasingly weak. Consequently, the magnetic ground state transforms from antiferromagnetism to ferrimagnetism, and the magnetic transition temperature increases. We propose the $5d^3$-$3d^5$ superexchange is intrinsically antiferromagnetic, instead of being, as previously thought, ferromagnetic. Our work illustrates the magnetic frustration can be effectively relieved by lattice distortion in certain $3d$–$5d$ ($4d$) double perovskites.

Methods

First-principles calculations. First-principles calculations based on DFT are performed within the generalized gradient approximation (GGA) according to the Perdew-Burke-Ernzerhof (PBE) parameterization as implemented in Vienna *Ab initio* Simulation Package (VASP)[30]. The projector-augmented wave
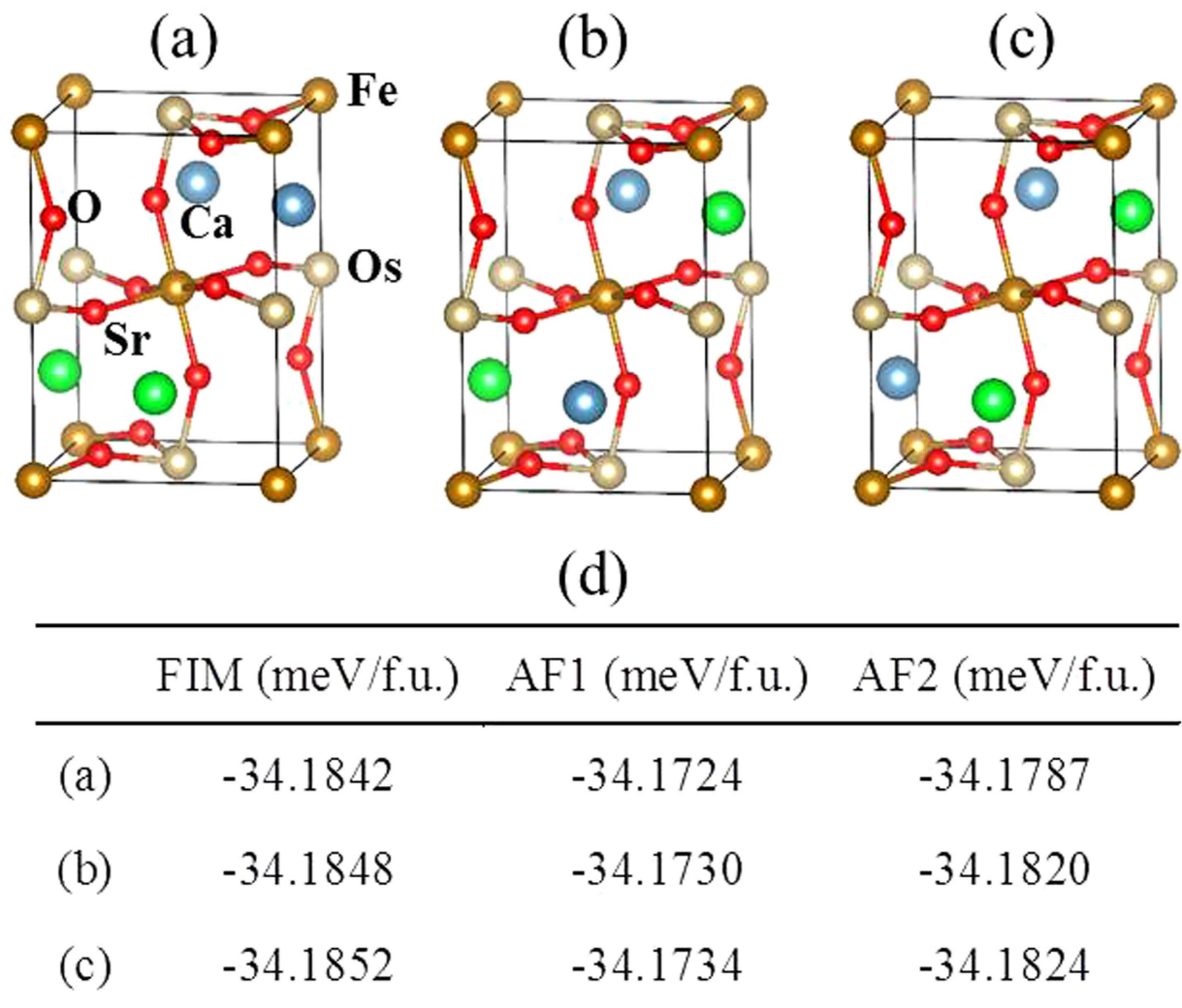
Figure 6. Three types of arrangement patterns of Ca²⁺ and Sr²⁺ ions in the SrCaFeOsO₆, and their corresponding energies. (**a**) All Ca²⁺ (Sr²⁺) are arranged in the *ab* plane. (**b**) All Ca²⁺ (Sr²⁺) are arranged along the *c* axis. Figure (**c**) shows Ca²⁺ and Sr²⁺ ions are arranged in the checkerboard manner. Figure (**d**) shows the energies of the FIM, AF1 and AF2 magnetic structures of the three most typical arrangement patterns of the Ca²⁺ and Sr²⁺ ions.

method[31], with an energy cutoff of 500 eV and a gamma-centered k-point mesh grid are used. Ion positions are relaxed towards equilibrium with the Hellmann-Feynman forces on each ion set to be less than 0.01 eV/Å. We use the simplified (rotationally invariant) coulomb-corrected density functional (DFT + U) method according to Dudarev *et al.*[32]. $U_{Fe}^{eff} = 4.0\,eV$, and $U_{Os}^{eff} = 2.0\,eV$ are applied to the Fe 3*d* and Os 5*d* states[22], respectively. With this effective U, the calculated band gap of Ca₂FeOsO₆ is about 1.19 eV, very close to the experimentally measured activation energy[7] $\left(E_{gap} = 1.2\,eV\right)$. Because the spin-orbit coupling (SOC) in Ca₂FeOsO₆ has been demonstrated to be insignificant[19], SOC is not taken into account in this present work.

Maximal localized Wannier functions calculations. Hopping integrals between 3*d*/5*d* orbitals are extracted from the real-space Hamiltonian matrix elements in the non-spin-polarized MLWFs basis. MLWFs are obtained by employing the **vasp2wannier90** interface in combination with the **wannier90** tool[33]. In order to obtain the 3*d*/5*d*-like Wannier functions, we construct MLWFs in a suitable energy window, using primarily 3*d*/5*d* antibonding states. All MLWFs are considered to be well converged if the total spread over 50 successive iterations is smaller than 10^{-9}Å².

Monte Carlo simulations. The magnetic phase transition temperature T_C or T_N is obtained using parallel tempering Monte Carlo simulations[34,35]. These calcuations are performed on the $7 \times 7 \times 5$

supercell based on the classical spin Hamiltonian: $H = \sum_{\langle i,j \rangle} J_{ij} \mathbf{S}_i \bullet \mathbf{S}_j$, wherein the spin exchange parameters J_{ij} are those defined in the text. To obtain the T_C or T_N, we first calculate the specific heat $C = \frac{(\langle E^2 \rangle - \langle E \rangle^2)}{T^2}$ once the system reaches equilibrium at a given temperature (T). Then T_N can be obtained by locating the maximum on the C(T) vs T plot.

References

1. Kobayashi, K. I., Kimura, T., Sawada, H., Terakura, K. & Tokura, Y. Room-temperature magnetoresistance in an oxide material with an ordered double-perovskite structure. *Nature* **395,** 677 (1998).
2. Erten, O. *et al.* Theory of Half-Metallic Ferrimagnetism in Double Perovskites. *Phys. Rev. Lett.* **107,** 257201 (2011).
3. Sarma, D. D., Mahadevan, P., Saha-Dasgupta, T., Ray, S. & Kumar, A. Electronic Structure of Sr_2FeMoO_6. *Phys. Rev. Lett.* **85,** 2549 (2000).
4. Erten, O. *et al.* Theory of half-metallic double perovskites. II. Effective spin Hamiltonian and disorder effects. *Phys. Rev. B* **87,** 7 (2013).
5. Meetei, O. N. *et al.* Theory of half-metallic double perovskites. I. Double exchange mechanism. *Phys. Rev. B* **87,** 7 (2013).
6. Krockenberger, Y. *et al.* Sr_2CrOsO_6: End point of a spin-polarized metal-insulator transition by 5d band filling. *Phys. Rev. B* **75,** 020404 (2007).
7. Feng, H. L. *et al.* High-Temperature Ferrimagnetism Driven by Lattice Distortion in Double Perovskite Ca_2FeOsO_6. *J. Am. Chem. Soc.* **136,** 3235 (2014).
8. Meetei, O. N., Erten, O., Randeria, M., Trivedi, N. & Woodward, P. Theory of High T_C Ferrimagnetism in a Multiorbital Mott Insulator. *Phys. Rev. Lett.* **110,** 087203 (2013).
9. Das, H., Sanyal, P., Saha-Dasgupta, T. & Sarma, D. D. Origin of magnetism and trend in T_C in Cr-based double perovskites: Interplay of two driving mechanisms. *Phys. Rev. B* **83,** 104418 (2011).
10. Sanyal, P. Ferromagnetism in Cr-based 3d-5d double perovskites: Effective model analysis and simulations. *Phys. Rev. B* **89,** 115129 (2014).
11. Azuma, M. *et al.* Designed ferromagnetic, ferroelectric Bi_2NiMnO_6. *J. Am. Chem. Soc.* **127,** 8889 (2005).
12. Goffinet, M., Iniguez, J. & Ghosez, P. First-principles study of a pressure-induced spin transition in multiferroic Bi_2FeCrO_6. *Phys. Rev. B* **86,** 6 (2012).
13. Yáñez-Vilar, S. *et al.* Multiferroic behavior in the double-perovskite Lu_2MnCoO_6. *Phys. Rev. B* **84,** 134427 (2011).
14. Nechache, R. *et al.* Epitaxial Patterning of Bi_2FeCrO_6 Double Perovskite Nanostructures: Multiferroic at Room Temperature. *Adv. Mater.* **23,** 1724 (2011).
15. Retuerto, M., Alonso, J., García-Hernández, M. & Martínez-Lope, M. Synthesis, structure and magnetic properties of the new double perovskite Ca_2CrSbO_6. *Solid State Commun.* **139,** 19 (2006).
16. Haskel, D. *et al.* Stability of the ferromagnetic ground state of La_2MnNiO_6 against large compressive stress. *Phys. Rev. B* **84,** 100403 (2011).
17. Guo, H. Z., Gupta, A., Varela, M., Pennycook, S. & Zhang, J. D. Local valence and magnetic characteristics of La_2NiMnO_6. *Phys. Rev. B* **79,** 4 (2009).
18. Morrow, R., Freeland, J. W. & Woodward, P. M. Probing the Links between Structure and Magnetism in $Sr_{2-x}Ca_xFeOsO_6$ Double Perovskites. *Inorg. Chem.* **53,** 7983 (2014).
19. Wang, H., Zhu, S., Ou, X. & Wu, H. Ferrimagnetism in the double perovskite Ca_2FeOsO_6: A density functional study. *Phys. Rev. B* **90,** 054406 (2014).
20. Paul, A. K. *et al.* Synthesis, Crystal Structure, and Physical Properties of Sr_2FeOsO_6. *Inorg. Chem.* **52,** 6713 (2013).
21. Paul, A. K. *et al.* Lattice Instability and Competing Spin Structures in the Double Perovskite Insulator Sr_2FeOsO_6. *Phys. Rev. Lett.* **111,** 167205 (2013).
22. Kanungo, S., Yan, B., Jansen, M. & Felser, C. *Ab initio* study of low-temperature magnetic properties of double perovskite Sr_2FeOsO_6. *Phys. Rev. B* **89,** 214414 (2014).
23. Kanamori, J. & Terakura, K. A general mechanism underlying ferromagnetism in transition metal compounds. *J. Phys. Soc. Jpn.* **70,** 1433 (2001).
24. Xiang, H., Lee, C., Koo, H.-J., Gong, X. & Whangbo, M.-H. Magnetic properties and energy-mapping analysis. *Dalton Transactions* **42,** 823 (2013).
25. Kugel, K. I. & Khomskii, D. I. Crystal-structure and magnetic properties of substances with orbital degeneracy. *Zhurnal Eksperimentalnoi I Teoreticheskoi Fiziki* **64,** 1429 (1973).
26. Kugel' KIi. & Khomskiĭ D. The Jahn-Teller effect and magnetism: transition metal compounds. *Physics-Uspekhi* **25,** 231 (1982).
27. Mazurenko, V. V., Mila, F. & Anisimov, V. I. Electronic structure and exchange interactions of $Na_2V_3O_7$. *Phys. Rev. B* **73,** 014418 (2006).
28. Kováčik, R. & Ederer, C. Calculation of model Hamiltonian parameters for $LaMnO_3$ using maximally localized Wannier functions. *Phys. Rev. B* **81,** 245108 (2010).
29. Goodenough, J. B. *Magnetism and the chemical bond* [183–184]. (Interscience Publishers, New York, 1963).
30. Perdew, J. P., Burke, K. & Ernzerhof, M. Generalized Gradient Approximation Made Simple. *Phys. Rev. Lett.* **77,** 3865 (1996).
31. Blöchl, P. E. Projector augmented-wave method. *Phys. Rev. B* **50,** 17953 (1994).
32. Dudarev, S. L., Botton, G. A., Savrasov, S. Y., Humphreys, C. J. & Sutton, A. P. Electron-energy-loss spectra and the structural stability of nickel oxide: An LSDA+U study. *Phys. Rev. B* **57,** 1505 (1998).
33. Mostofi, A. A. *et al.* wannier90: A tool for obtaining maximally-localised Wannier functions. *Comput. Phys. Commun.* **178,** 685 (2008).
34. Hukushima, K. & Nemoto, K. Exchange Monte Carlo Method and Application to Spin Glass Simulations. *J. Phys. Soc. Jpn.* **65,** 1604 (1996).
35. Wang, P. S. & Xiang, H. J. Room-Temperature Ferrimagnet with Frustrated Antiferroelectricity: Promising Candidate Toward Multiple-State Memory. *Phys. Rev. X* **4,** 011035 (2014).

Author Contributions

Y.H. contributed to the "first-principle" calculations and writing of the article. H.X. contributed to the discussion of results and the manuscript refinement. X.G. suggested the form of the calculations, and also contributed significantly to the discussion of results and refinement of the manuscript.

Additional Information